Electronic Structure

OPEN ACCESS

RECEIVED
9 October 2020

REVISED
12 December 2020

ACCEPTED FOR PUBLICATION
17 December 2020

PUBLISHED
7 January 2021

PAPER

Zero-point energies prevent a trigonal to simple cubic transition in high-pressure sulfur

Jack Whaley-Baldwin *

TCM Group, Cavendish Laboratory, University of Cambridge, United Kingdom

* Author to whom any correspondence should be addressed.

E-mail: jajw4@cam.ac.uk

Keywords: high pressure, structure searching, phase transition, solid sulfur, phonons, anharmonic vibrations

Abstract

Recently published density functional theory results using the PBE functional (Whaley-Baldwin and Needs 2020 *New J. Phys.* 22 023020) suggest that elemental sulfur does not adopt the simple-cubic (SC) $Pm\bar{3}m$ phase at high pressures, in disagreement with previous works (Rudin and Liu 1999 *Phys. Rev. Lett.* **83** 3049–52; Gavryushkin *et al* 2017 *Phys. Status Solidi* B **254** 1600857). We carry out an extensive set of calculations using a variety of different exchange–correlation functionals (both local and non-local), and show that even though under LDA and PW91 a high-pressure SC phase does indeed become favourable at the static lattice level, when zero-point energies (ZPEs) are included, the transition to the SC phase is suppressed in every case, owing to the larger ZPE of the SC phase; thus confirming the transition sequence as $R\bar{3}m \rightarrow$ BCC, with no intervening SC phase. We reproduce these findings with pseudopotentials that explicitly include core electronic states, and show that even at these high pressures, only the $n = 3$ valence shell contributes to bonding in sulfur. We then compare our findings against the all-electron code ELK, which is in excellent agreement with our pseudopotential results, and examine the roles of the exchange and correlation contributions to the total energy. We further calculate anharmonic vibrational corrections to the ZPEs of the two phases, and find that such corrections are several orders of magnitude smaller than the ZPEs and are thus negligible. The effect of finite temperatures is also considered, and we show that the $Pm\bar{3}m$ phase becomes even more unfavourable with an increase in temperature. Finally, the experimental consequences of our results on the equation of state of sulfur and its superconducting critical temperature are explicitly calculated.

1. Introduction

High-pressure first-principles investigations on sulfur [1–3] have identified primitive simple-cubic (SC) $Pm\bar{3}m$ sulfur as an energetically competitive phase in the range 300–500 GPa, where it competes with a single-atom trigonal $R\bar{3}m$ phase. Using the LDA [4] and PBE [5] exchange–correlation functionals, previous authors have concluded that a transition to the $Pm\bar{3}m$ phase occurs at around 280 GPa [2, 3], whereas [1] finds (using PBE) that the SC phase is not favourable at either the static-lattice or zero-point energy (ZPE)-included level of theory. All three authors are however in agreement that sulfur eventually adopts a primitive BCC Im $\bar{3}m$ structure at a pressure of around 500 GPa.

The existence of a SC phase in sulfur would be significant, as the $Pm\bar{3}m$ space group is, even at high pressures, only rarely encountered among elemental crystal structures [6] as a lowest-enthalpy phase, primarily due to its highly unfavourable packing efficiency.

2. Computational details

We used version 19.1 of the plane-wave DFT code CASTEP [7] for our electronic structure calculations. A Fermi–Dirac electronic smearing temperature of 500 K and a k-point spacing of 0.01 Å^{-1} (giving ≈3000 k

Table 1. Details of the different pseudopotentials used in this study. R_c is the cutoff radius for each pseudopotential (chosen to be the same for all projectors) and l_{loc} is the local channel. 'NC' denotes that a norm-conserving pseudopotential was used.

Projectors and Functional	R_c (Bohr)	l_{loc}	Cutoff (eV)
3*s*3*p*3*d*, LDA	1.6	3	800
2*s*2*p*3*s*3*p*3*d*, LDA	1.6	3	1000
3*s*3*p*3*d*, B3LYP (NC)	1.6	3	1000
3*s*3*p*3*d*, PW91	1.6	3	800
3*s*3*p*3*d*, PBE	1.6	3	800
3*s*3*p*3*d*, PBE0 (NC)	1.6	3	1000
3*s*3*p*3*d*, PBESOL	1.6	3	800
3*s*3*p*3*d*, WC91	1.6	3	800

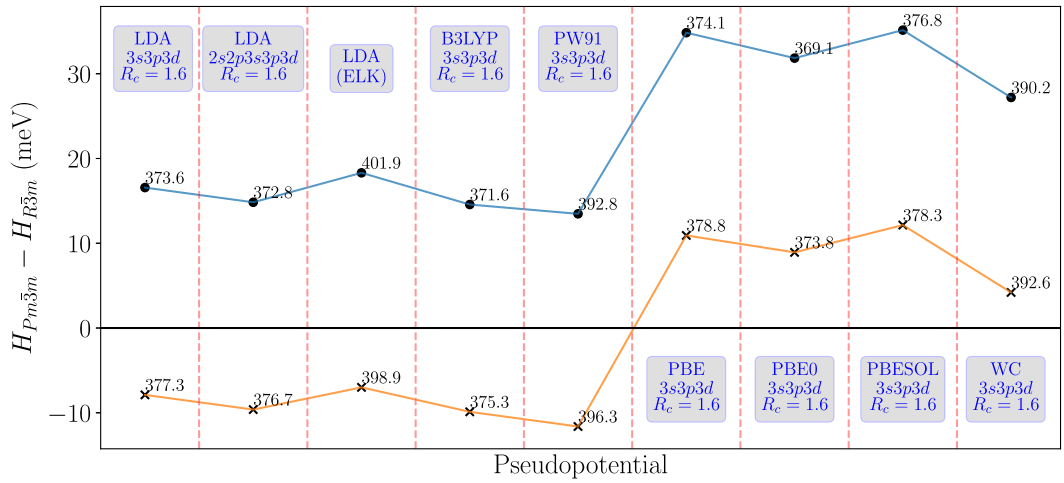

Figure 1. Enthalpy of the SC $Pm\bar{3}m$ phase of sulfur relative to the trigonal $R\bar{3}m$ phase using different functionals and pseudopotentials. Crosses denote static lattice enthalpies, and filled-in circles denote static lattice enthalpies with ZPEs included. The pressure at which the SC phase is lowest in energy relative to the $R\bar{3}m$ phase is shown next to each datapoint. The lines are a guide to the eye. Note: The ELK code does not use pseudopotentials, but rather is an all-electron code.

points in $Pm\bar{3}m$ sulfur at 350 GPa) was used throughout. All geometry optimisations were carried out such that the force on each atom was less than 1×10^{-5} eV Å^{-1}, and the differential stress on each unit cell less than 1×10^{-4} GPa.

In this study, we considered a variety of different pseudopotentials and XC-functionals (both local and non-local), which are detailed in table 1. The plane-wave cutoff values specified in the table were sufficient to converge the absolute energy of each pseudopotential to better than ±0.5 meV, with the relative convergence between structures being even better than this [see supplemental material (https://stacks.iop.org/EST/2/045003/mmedia)].

The study of high-pressure phases of matter with codes that employ pseudopotentials require careful consideration. Most notably, it is essential that (i) the cutoff radius of the pseudopotentials, when doubled, is appreciably smaller than the smallest bond length (s) and (ii) the correct number of valence electrons are included, which may require, in the definition of the pseudopotential, the inclusion of semi-core states. Including projections onto higher-energy states (which, although unoccupied in the isolated atom, become (partially) occupied in the crystal) may also be important.

We used mostly ultrasoft pseudopotentials [8], although norm-conserving pseudopotentials [9] were used for the non-local B3LYP and PBE0 functionals. The pseudopotentials were created using the CASTEP on-the-fly-generation (OTFG) program which is bundled with the code. We used two ultrasoft projectors per orbital in all of the pseudopotential definitions, except for the 2*s*2*p*3*s*3*p*3*d* pseudopotential, where only one projector was used for each of the 2*s* and 2*p* orbitals. All of the cutoff radii in table 1 are less than half the smallest interatomic separation in this study (≈1.82 Å in SC sulfur at 525 GPa).

The choice of pseudopotentials in table 1 reflects a variety of XC-functionals. For the LDA case only, we constructed an extra pseudopotential that explicitly included the core $n = 2$ states as valence, in order to check whether the $n = 2$ shell contributes to bonding, and thus to the enthalpy difference between the phases. As will be discussed later, and as demonstrated in figure 1, the $n = 2$ shell actually had a negligible effect on our results.

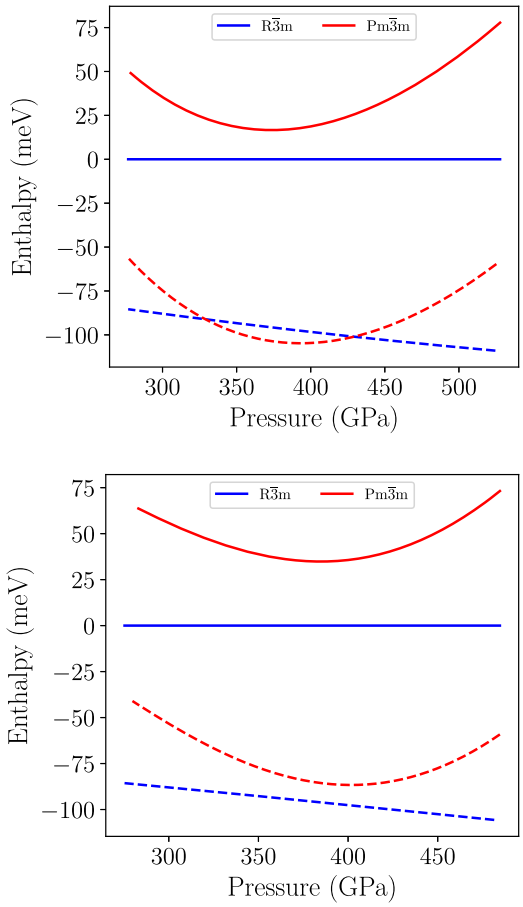

Figure 2. Relative enthalpy curves for the SC and trigonal phases of sulfur using the LDA functional (top) and PBE functional (bottom). Dotted lines denote energies without ZPEs, solid lines are with ZPEs included. The PW91 functional enthalpy curve is very similar to the top plot, and the PBESOL and WC enthalpy curves are very similar to the bottom plot.

We additionally compare our CASTEP LDA results to those of the all-electron code ELK [10], which utilises the full-potential linearised augmented plane wave (FLAPW) method. A fixed muffin-tin radius of 1.788 Bohr was used for the ELK calculations and the basis set size parameter $R_{\mathrm{MT}} \times \max\{\vec{G}, \vec{k}\} = 9$, with a $50 \times 50 \times 50k$-point grid used throughout. The interstitial density was expanded with $|\vec{G}_{\mathrm{max}}| = 14$ Bohr. Since the ELK code cannot presently perform non-zero externally applied stress geometry optimisations, the output geometry of the $2s2p3s3p3d$ CASTEP calculation (see table 1) was fed into the ELK calculation, and ELK was simply used to evaluate total energies.

Harmonic phonon calculations were carried out using the finite-differences method within the vert CASTEPvert code and density functional perturbation theory (DFPT) within the ELK code. A $4 \times 4 \times 4q$-point grid was used in both cases.

The final total energy $E_{\mathrm{tot}} = E_{\mathrm{elec}} + E_{\mathrm{phonon}}$ and volume values from each optimisation were taken and fitted to the Vinet equation of state [11]. The enthalpy was then derived from the derivative of this curve as $H = E - V\left(\frac{\partial E}{\partial V}\right)_T$. This approach therefore includes the (harmonic) phonon contribution to the total pressure.

3. Energies of the trigonal and SC phases

Figure 2 shows relative enthalpy curves (at 0 K) for the $Pm\bar{3}m$ and $R\bar{3}m$ phases of sulfur using the LDA and PBE exchange–correlation functionals, both with and without the inclusion of ZPEs. Within the LDA, a transition from the $R\bar{3}m$ to the $Pm\bar{3}m$ phase occurs at the static lattice level, but this transition is suppressed when ZPEs are included. Using PBE, no transition occurs either with or without ZPEs. The PW91 [12] curve has a shape identical to that of the LDA case with slightly shifted values, and likewise the PBESOL [13] and WC [14] curves have shapes identical to that of the PBE curve with shifted values.

Figure 1 shows the smallest calculated enthalpy of the SC phase relative to the trigonal phase for a variety of pseudopotentials and exchange–correlation functionals. It can be seen, using LDA and PW91, that on average the SC phase is lower in energy at the static lattice level by around 9 meV. On the other hand, PBE, PBESOL

Table 2. Decomposition of the total energy (in eV) of the $Pm\bar{3}m$ phase relative to the $R\bar{3}m$ phase, according to LDA and PBE, at 375 GPa. The last row is the difference in each contribution between the two functionals. The Coulomb term is the sum of the Hartree, nuclear–nuclear and electron–nuclear terms. T_s is the electron kinetic energy. E_X and E_C represent the exchange and correlation energies, respectively. E_{tot} is the sum of all contributions.

Functional	$E_{Coulomb}$	T_s	E_X	E_C	E_{tot}
LDA	0.9850	−0.1760	−0.7758	−0.0389	−0.0057
PBE	1.0193	−0.2005	−0.8958	0.0937	0.0167
(LDA–PBE)	−0.0343	0.0245	0.1200	−0.1326	−0.0224

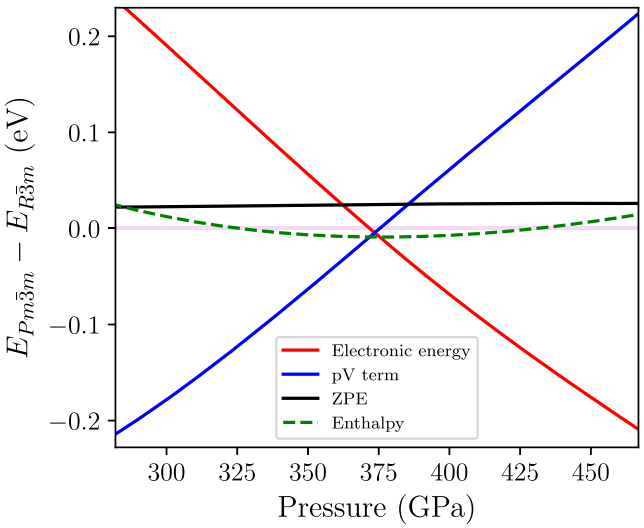

Figure 3. 0 K electronic energy, the pV term, phonon ZPE and static-lattice enthalpy H of the $Pm\bar{3}m$ phase relative to the $R\bar{3}m$ phase using LDA. Data was taken in 25 GPa intervals and fitted to a cubic spline. A faint horizontal line at $E = 0$ has been drawn for clarity.

and WC have that the SC phase is higher in energy at the static lattice level, by around 10 meV for the PBE and PBESOL cases, and around 4 meV for the WC case. When ZPEs are included however, the enthalpy of the SC phase relative to the $R\bar{3}m$ phase is higher in every single case by at least 12 meV, rising to 35 meV for the PBE case.

Table 2 shows, at 375 GPa, why the total electronic energy of the $Pm\bar{3}m$ phase becomes favourable according to LDA but not PBE. Although the exchange energy is larger, there is a correspondingly greater decrease in the correlation energy when moving to LDA from PBE, thus reducing the overall exchange–correlation energy. The total Coulomb energy is also reduced significantly when moving from LDA to PBE. While there is an increase in the electronic kinetic energy T_s, this is not enough to offset the gains made by the reduction in the XC and Coulomb terms, and thus the $Pm\bar{3}m$ phase has a favourable electronic energy according to the LDA.

Figure 3 decomposes the contributions to the overall enthalpy of each phase within the LDA. It shows that the $Pm\bar{3}m$ phase becomes energetically favourable at the static lattice level because, below 375 GPa, its electronic energy falls (for reasons discussed in the previous paragraph) more quickly than the increase in its pV term. This results in a relative static-lattice enthalpy reduction that reaches a maximum of ≈9 meV at 375 GPa, with the benefit reducing above this pressure. The ZPE of the $Pm\bar{3}m$ phase is, however, consistently higher than that of the $R\bar{3}m$ phase throughout; slowly increasing from 22.3 meV to 26.1 meV between 280 and 470 GPa respectively. It is the failure of the static-lattice enthalpy reduction to offset the large difference in ZPE that prevents the $Pm\bar{3}m$ from becoming the ground state of sulfur at these pressures.

Figure 4 reveals why the ZPE of the SC phase is significantly higher than that of the trigonal phase. Whereas the $R\bar{3}m$ phonon density of states (DOS) plot is shaped approximately like a uniform top-hat function between 200 and 900 cm^{-1}, the cubic $Pm\bar{3}m$ DOS curve has most of its weight above 600 cm^{-1}, with a pronounced peak at ≈950 cm^{-1}. The $Pm\bar{3}m$ DOS curve also extends to higher energies than the $R\bar{3}m$ curve. These result

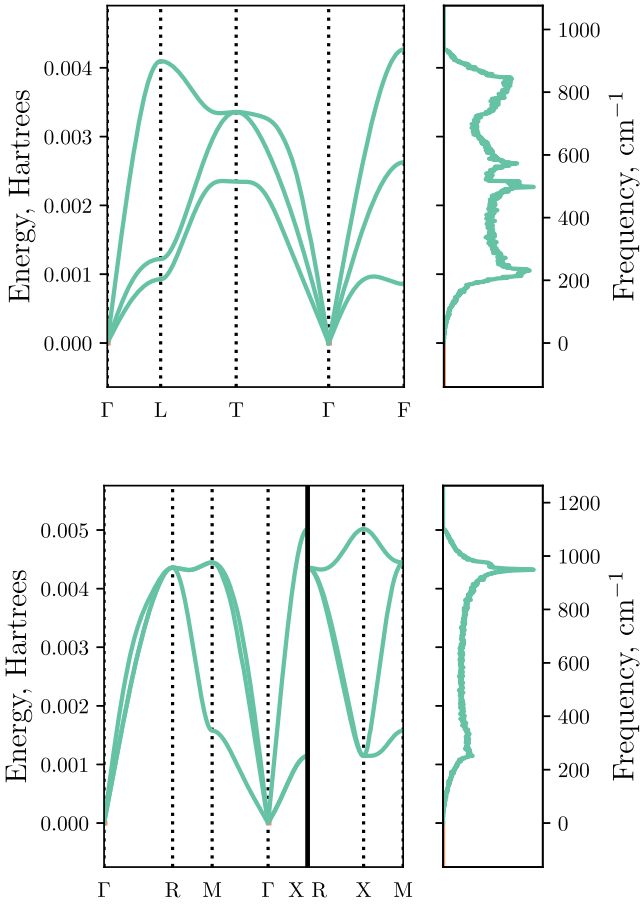

Figure 4. Phonon dispersion curves for the trigonal $R\bar{3}m$ phase of sulfur (top) and the SC $Pm\bar{3}m$ phase (bottom) at 375 GPa using LDA. The high-symmetry points are labeled according to standard convention for the (primitive) trigonal and cubic cells, respectively. The phonon DOS is shown in a panel on the right of each plot.

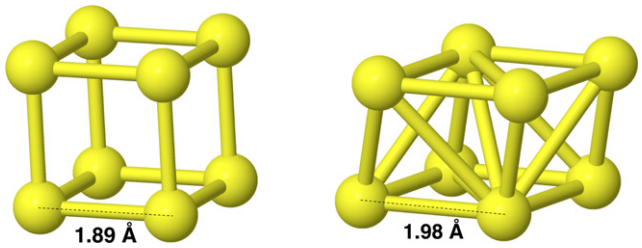

Figure 5. The primitive $Pm\bar{3}m$ SC (left) and primitive $R\bar{3}m$ trigonal structures of sulfur at 350 GPa according to the LDA. The rhombohedral lattice angle for the trigonal structure is 104.9°.

in a lower ZPE, which is given by the integral:

$$E_{\mathrm{ZPE}} = \frac{1}{2}\int \omega g(\omega)\mathrm{d}\omega \tag{1}$$

Where $g(\omega)$ is the phonon DOS. As first pointed out by [2], the hardening of the phonon modes in the $Pm\bar{3}m$ phase is primarily a result of the shorter bond lengths in this structure (see figure 5).

At finite temperatures, where the quantity determining phase stability is the Gibbs free energy $G(p, T)$, the stability of the $R\bar{3}m$ phase is enhanced, as the minimum Gibbs free energy gap between the phases (occurring at around 375 GPa with LDA) increases from its 0 K value of 15 meV up to 50 meV at 1000 K under the harmonic approximation (the *quasi*-harmonic approximation (QHA) was not employed). This is because the phonon free energy $F_{\mathrm{ph}}(T, V)$ for the $Pm\bar{3}m$ phase rises more rapidly than that of the $R\bar{3}m$ phase, owing to the much greater number of low-frequency vibrational modes in the $R\bar{3}m$ case (see figure 4). $G(p, T)$ is plotted in figure 6. Using the PBE, PBESOL or WC functionals, the Gibbs free energy gap at any given temperature is even larger.

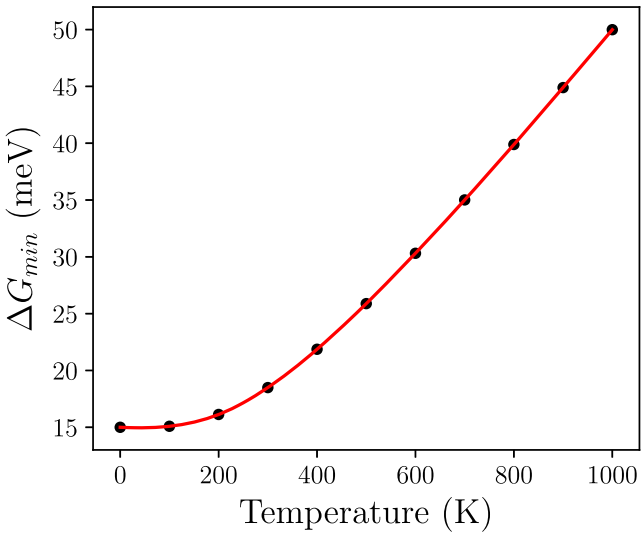

Figure 6. The minimum Gibbs free energy gap in meV, $\Delta G_{\text{min}}(T) \equiv G_{Pm\bar{3}m}(T) - G_{R\bar{3}m}(T)$, between the SC and trigonal phases within the harmonic approximation using the LDA functional, plotted as a function of temperature.

4. Anharmonic corrections to ZPEs

Having established that the trigonal → SC transition does not occur for any XC-functional at the harmonic level, we considered whether anharmonic corrections to the ZPEs of the $Pm\bar{3}m$ and $R\bar{3}m$ structures would result in a transition with the LDA functional. This would occur if the anharmonic corrections were such that the large energy difference between the ZPEs was reduced significantly.

We first computed the harmonic phonons on a $6 \times 6 \times 6$ q-point grid, and then used a coarser $2 \times 2 \times 2$ q-point grid for the anharmonic calculations. Corrections up to quartic order in the vibrational Hamiltonian were considered, but we did not include any cross-coupling terms between non-degenerate phonon modes. This means that the vibrational Hamiltonian contained terms such as q_1^3, q_2^3, q_1^4, q_2^4, $q_1^3 q_2$, $q_1^2 q_2^2$ etc (where the q_i are phonon normal mode coordinates, and modes 1 and 2 are degenerate), but not, for example, $q_1^3 q_3$ if modes 1 and 3 are not degenerate.

It was found that at 375 GPa (the pressure at which the enthalpy gap between the phases is lowest under LDA) the ZPE of the $Pm\bar{3}m$ structure decreases by 0.272 meV, and that of the $R\bar{3}m$ structure decreases by 0.218 meV. This gives an overall relative ZPE change of 0.054 meV, which is several orders of magnitude smaller than the minimum enthalpy gap between the phases at the harmonic level (15 meV). Therefore, the inclusion of anharmonic corrections to the ZPEs does not change our conclusions.

These findings also demonstrate that sulfur is strongly harmonic even at these large pressures.

5. Electronic DOS

Figure 7 shows electronic DOS plots for the trigonal and SC phases at 375 GPa using LDA, where the static-lattice enthalpy of the SC phase relative to the trigonal phase is lowest.

In comparison to the trigonal phase, the $Pm\bar{3}m$ phase total DOS has a greater weight at lower energies, which lowers the total electronic energy. The Fermi energy E_{F} is also very slightly lowered in the $Pm\bar{3}m$ phase compared to the trigonal phase. These effects become more pronounced with increasing pressure, hence the negative slope of the red line in figure 3. As discussed, while this relative electronic energy gain is enough to overcome the contribution of the pV term in a certain pressure window, it is not large enough to overcome the much larger ZPE of the SC phase.

6. Hybrid functionals

Hybrid functionals (partially) incorporate exact exchange into the exchange–correlation functional.

We have further investigated the relative stability of the $R\bar{3}m$ and $Pm\bar{3}m$ phases using the B3LYP [15] and PBE0 [16] non-local functionals, the results of which are shown in figure 1.

Compared to LDA, the $Pm\bar{3}m$ phase is slightly more favourable at the static lattice level (by $\approx$3 meV) when using B3LYP, although once again, when ZPEs are included, the trigonal phase is favored. Similarly, when using

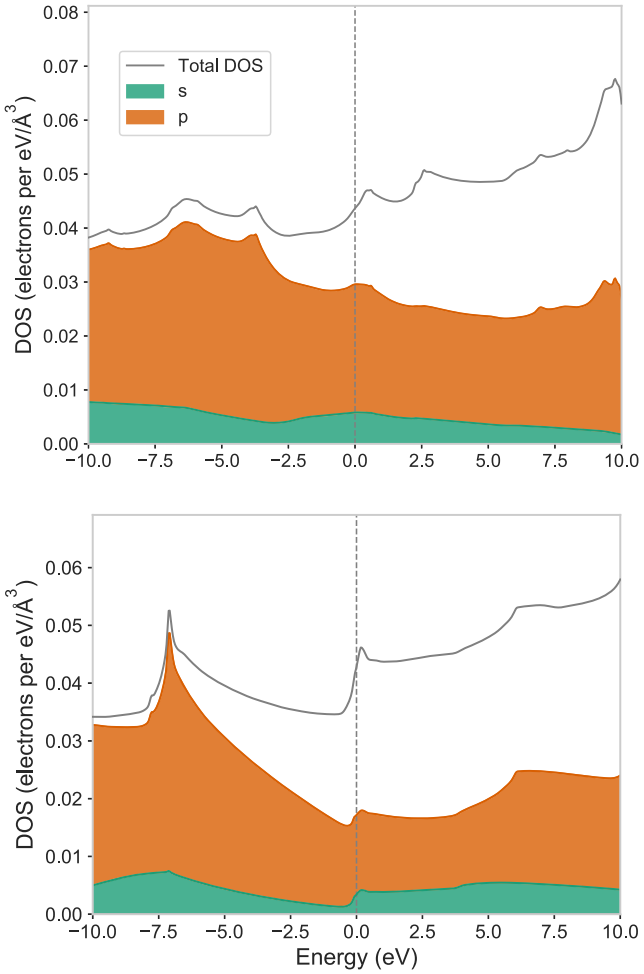

Figure 7. Electronic total and partial DOS plots for the $R\bar{3}m$ phase (top) and $Pm\bar{3}m$ phase (bottom) at 375 GPa. The projections onto the $l = 0$ channel are shown in green, and onto the $l = 1$ channel in orange. The Fermi level is set at $E = 0$.

PBE0, the $Pm\bar{3}m$ phase is reduced in enthalpy compared to when using PBE, although the change is again just a few meV, which is not enough to change our conclusions.

7. Effects on equation of state

Figure 8 shows the volume of the trigonal and SC phases of sulfur as a function of pressure, and shows that a volume discontinuity would occur upon transition to the $Pm\bar{3}m$ phase if it were indeed favourable.

As we have shown, the $R\bar{3}m \rightarrow Pm\bar{3}m$ transition does not occur when ZPEs are considered, and so the discontinuity does not occur in practice, implying that the pV curve of sulfur is continuous over this pressure range. This observation should also provide a convenient means to verify our predictions in experiment.

8. Superconducting critical temperatures

A significant consequence of the persistence of the $R\bar{3}m$ phase is that a marked drop in the superconducting critical temperature of sulfur from $\approx$12.5 K to $\approx$6 K, that would otherwise occur upon transition to the $Pm\bar{3}m$ phase [2], is prevented.

Figure 9 shows the superconducting critical temperature T_c as a function of pressure for the SC and trigonal phases, as calculated using the McMillan-Allen-Dynes formula [17] within DFPT using the vert quantum ESPRESSOvert code [18]. Our procedure for calculating T_c is detailed in the supplemental material. For comparison, the T_c of sulfur in the $R\bar{3}m$ phase has been calculated to be 15 K at 231 GPa [19], although sulfur has not yet been taken beyond this pressure in experiment.

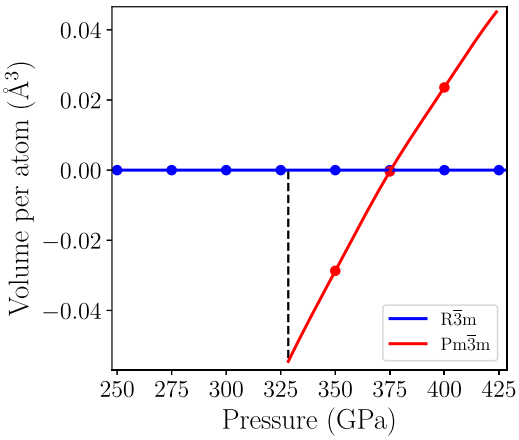

Figure 8. Volume per atom as a function of pressure according to LDA at the static lattice level, normalised to the volume of the $R\bar{3}m$ structure. A dotted vertical line indicates the static-lattice phase transition according to LDA.

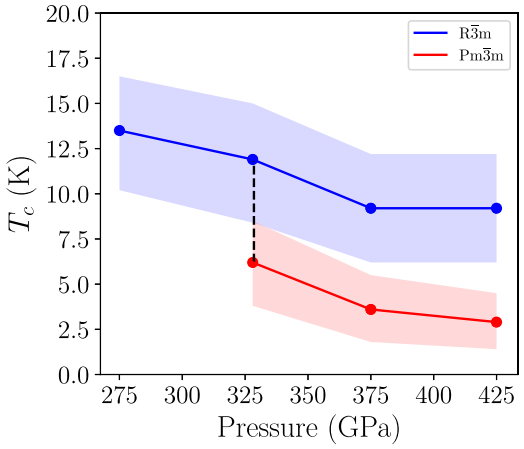

Figure 9. Superconducting critical temperatures of the $R\bar{3}m$ and $Pm\bar{3}m$ phases as a function of pressure. A dotted vertical line indicates the static-lattice phase transition according to LDA. The width of the lines corresponds to values of the Coulomb pseudopotential parameter [17] in the range $\mu \in [0.1, 0.15]$.

9. Conclusions

We have shown using a variety of XC-functionals that the high-pressure trigonal → SC transition does not take place in sulfur when ZPEs are included, and we have further shown that neither the explicit addition of core ($n = 2$) electrons, nor the consideration of anharmonic corrections to the ZPEs, are able to change this conclusion. The transition becomes even less favourable at finite temperatures.

The SC phase becomes favourable at the static-lattice level under LDA and PW91 due to its lower electronic energy as a result of a reduced Coulomb and exchange–correlation energy. However, its comparatively much larger ZPE relative to the $R\bar{3}m$ phase suppresses the transition. This result is the same when non-local functionals such as B3LYP and PBE0, which incorporate exact exchange, are considered.

We have investigated the consequences of our results for the high-pressure equation of state of sulfur, as well as sulfur's superconducting critical temperature, showing that a previously predicted [2] reduction in T_c should not occur.

As mentioned in the concluding remarks of [1], experimental work is needed to confirm these findings. The highest pressures to be considered (≈500 GPa) lie within those accessible by high-pressure diamond anvil experiments, and this pressure should also be sufficient to confirm the subsequent transition to the BCC phase.

Acknowledgments

The author wishes to thank Mark Johnson, Michael Hutcheon and Stewart Clark for useful discussions. The author acknowledges funding via an EPSRC studentship. The computational resources for this project were provided by the Cambridge Service for Data Driven Discovery (CSD3). The author is further grateful for computational support from the UK national high performance computing service, ARCHER, for which access was obtained via the UKCP consortium and funded by EPSRC Grant ref EP/P022561/1.

ORCID iDs

Jack Whaley-Baldwin https://orcid.org/0000-0001-9350-7115

References

[1] Whaley-Baldwin J and Needs R 2020 First-principles high pressure structure searching, longitudinal-transverse mode coupling and absence of simple cubic phase in sulfur *New J. Phys.* **22** 023020
[2] Rudin S P and Liu A Y 1999 Predicted simple-cubic phase and superconducting properties for compressed sulfur *Phys. Rev. Lett.* **83** 3049–52
[3] Gavryushkin P N, Litasov K D, Dobrosmislov S S and Popov Z I 2017 High-pressure phases of sulfur: topological analysis and crystal structure prediction *Phys. Status Solidi* B **254** 1600857
[4] Perdew J P and Zunger A 1981 Self-interaction correction to density-functional approximations for many-electron systems *Phys. Rev.* B **23** 5048–79
[5] Perdew J P, Burke K and Ernzerhof M 1996 Generalized gradient approximation made simple *Phys. Rev. Lett.* **77** 3865–8
[6] Urusov V S and Nadezhina T N 2009 Frequency distribution and selection of space groups in inorganic crystal chemistry *J. Struct. Chem.* **50** 22–37
[7] Clark S J, Segall M, Pickard C J, Hasnip P, Probert M, Refson K and Payne M C 2005 First principles methods using castep *Z. Kristallogr.* **220** 05
[8] Vanderbilt D 1985 Optimally smooth norm-conserving pseudopotentials *Phys. Rev.* B **32** 8412–5
[9] Hamann D R, Schlüter M and Chiang C 1979 Norm-conserving pseudopotentials *Phys. Rev. Lett.* **43** 1494–7
[10] Dewhurst J K *et al Elk code* http://elk.sourceforge.net/faq.html
[11] Vinet P, Smith J R, Ferrante J and Rose J H 1987 Temperature effects on the universal equation of state of solids *Phys. Rev.* B **35** 1945–53
[12] Perdew J P, Chevary J A, Vosko S H, Jackson K A, Pederson M R, Singh D J and Fiolhais C 1992 Atoms, molecules, solids, and surfaces: applications of the generalized gradient approximation for exchange and correlation *Phys. Rev.* B **46** 6671–87
[13] Perdew J P, Ruzsinszky A, Csonka G I, Vydrov O A, Scuseria G E, Constantin L A, Zhou X and Burke K 2008 Restoring the density-gradient expansion for exchange in solids and surfaces *Phys. Rev. Lett.* **100** 136406
[14] Wu Z and Cohen R E 2006 More accurate generalized gradient approximation for solids *Phys. Rev.* B **73** 235116
[15] Lee C, Yang W and Parr R G 1988 Development of the colle-salvetti correlation–energy formula into a functional of the electron density *Phys. Rev.* B **37** 785–9
[16] Perdew J P, Ernzerhof M and Burke K 1996 Rationale for mixing exact exchange with density functional approximations *J. Chem. Phys.* **105** 9982–5
[17] Allen P B and Dynes R C 1975 Transition temperature of strong-coupled superconductors reanalyzed *Phys. Rev.* B **12** 905–22
[18] Giannozzi P *et al* 2009 Quantum ESPRESSO: a modular and open-source software project for quantum simulations of materials *J. Phys.: Condens. Matter* **21** 395502
[19] Gregoryanz E, Struzhkin V V, Hemley R J, Eremets M I, Mao H-k. and Timofeev Y A 2002 Superconductivity in the chalcogens up to multimegabar pressures *Phys. Rev.* B **65** 064504